J. Biochem. **142,** 183–191 (2007)
doi:10.1093/jb/mvm121

Model-based Definition of Population Heterogeneity and Its Effects on Metabolism in Sporulating *Bacillus subtilis*

Mineo Morohashi[1], Yoshiaki Ohashi[1,2,*], Saeka Tani[2], Kotaro Ishii[2,†], Mitsuhiro Itaya[2], Hideaki Nanamiya[3,†], Fujio Kawamura[3], Masaru Tomita[1,2] and Tomoyoshi Soga[1,2]

[1]Human Metabolome Technologies, Inc., Tsuruoka, Yamagata 997-0052, Japan; [2]Institute for Advanced Biosciences, Keio University, Tsuruoka, Yamagata 997-0017, Japan; and [3]College of Science, Rikkyo (St Paul's) University, Toshima-ku, Tokyo 171-8501, Japan

Received April 1, 2007; accepted May 11, 2007; published online June 1, 2007

The soil bacterium *Bacillus subtilis* forms dormant, robust spores as a tactic to ensure survival under conditions of starvation. However, the sporulating culture includes sporulating and non-sporulating cells, because a portion of the cell population initiates sporulation in wild-type strain. We anticipated that the population effect must be considered carefully to analyse samples yielding population heterogeneity. We first built a mathematical model and simulated for signal transduction of the sporulation cue to see what mechanisms are responsible for generating the heterogeneity. The simulated results were confirmed experimentally, where heterogeneity is primarily modulated by negative feedback circuits, resulting in generation of a bistable response within the sporulating culture. We also confirmed that mutants relevant to negative feedback yield either sporulating or non-sporulating subpopulations. To see the effect of molecular mechanism between sporulating and non-sporulating cells in distinct manner, metabolome analysis was conducted using the above mutants. The metabolic profiles exhibited distinct characteristics with time regardless of whether sporulation was initiated or not. In addition, several distinct characteristics of metabolites were observed between strains, which was inconsistent with previously reported data. The results imply that careful consideration must be made in the interpretation of data obtained from cells yielding population heterogeneity.

Key words: Bacillus subtilis, heterogeneity, metabolome, sporulation.

Abbreviations: ANOVA, analysis of variance; CE-TOFMS, capillary electrophoresis time-of-flight mass spectrometry; PCA, principal component analysis.

Phenotypic heterogeneity in clonal populations has been found in some species of bacteria under certain circumstances (*1*–*3*). The soil bacterium *Bacillus subtilis* can form population heterogeneity during sporulation under conditions of starvation (*4*–*7*). This is achieved by functions of positive- and negative-feedback loops in sporulation signal transduction. In cells receiving a sporulation signal, the phosphorylation of kinases (such as KinA) is stimulated and the phosphate group is transferred to Spo0A *via* phosphorelay (*8*). Phosphorylated Spo0A (Spo0A~P) is a master regulator of sporulation, acting as a transcriptional factor for sporulation-associated genes. This signal transduction system is regulated by a complex mechanism involving multiple positive/negative-feedback loops (*9*).

Recent theoretical and experimental studies suggest that intrinsic characteristics of the biological system generate population heterogeneity [see (*10*) for a review]. Voigt *et al*. (*11*) investigated the dynamics of *sin* operon using a mathematical model, and showed that combining genes from a regulatory protein and its antagonist within the same operon could lead to diverse regulatory functions such as bistability, oscillation and pulse generation. In addition, Iber *et al*. (*12*, *13*) used the *spo*IIA operon as an example to show similar results while de Jong *et al*. (*9*) performed a qualitative simulation, reproducing qualitative characteristics consistent with these experimental results. Involvement of each genetic feedback loop is unquestionable, but how to modulate the scale of subpopulations is still unclear.

It has been a long time since omic approaches were introduced to investigate cellular dynamics. However, influence of population heterogeneity on omic data has never been discussed. We consider that lack of understanding regarding population heterogeneity mislead and complicate the interpretations of omic data.

Here we indicate that the population heterogeneity cannot be ignored in sporulation of *B. subtilis* population. At first, we employed a mathematical model to elucidate the dynamics of Spo0A~P, including the involvement of both positive and negative feedbacks. Although experimental data cannot be obtained from quantitative

*To whom correspondence should be addressed. Tel: +81-235-25-1447, Fax: +81-235-25-1450,
E-mail: ohashi@humanmetabolome.com/ohashi@sfc.keio.ac.jp
†Present addresses: Kotaro Ishii, The University of Tokyo, Kashiwa, Chiba 277-0000, Japan; Hideaki Nanamiya, Ehime University, Matsuyama, Ehime 790-8577, Japan.

simulation, the model allows us to investigate the essential functions of sporulation-relevant signal transduction pathways. Given the variation in sporulation signal intensity, Spo0A∼P exhibited unstable dynamics under specific conditions, corresponding to sporulation and non-sporulating subpopulations, respectively. Next, we confirmed that negative feedback primarily modulates the system dynamics, and alteration of negative feedback totally shifts the subpopulations to sporulate either 0 or 100%. The results were verified experimentally in *B. subtilis* by virtually activating/inhibiting factors of negative feedback.

To investigate the molecular mechanisms during sporulation, we anticipate that those controlled subpopulations (either sporulating or non-sporulating) must be examined, and not wild-type which contains both sporulating and non-sporulating cells. To test the hypothesis, we conducted metabolome analysis using the mutants above. The results revealed that metabolome profiles were distinct between strains, and even clear trajectories at each sampling time were obtained when principal component analysis (PCA) was conducted. Comparing two mutants (either sporulating or non-sporulating), we found several interesting characteristics in sporulation subpopulations. In particular, ATP and GTP exhibited a sharp increase during sporulation, but not in non-sporulating cells, suggesting accumulation of energy in the former. The result is inconsistent with reported data, implying that the past data may reflect mixture of sporulating and non-sporulating cells, possibly averaging the data. Given the results, we warn that careful experimental design must be followed in order to avoid misleading data interpretation against cells yielding population heterogeneity.

MATERIALS AND METHODS

Plasmids and Bacterial Strains—The bacterial strains used in this study are summarized in Table 1. The P_{spoVG}-*GFPuv* reporter gene (encoding green fluorescent protein) was constructed as follows. A polymerase chain reaction (PCR) product containing the *GFPuv* structural gene was introduced into the *Eco*RV site of pHASH103 (*14*) using the TA-cloning method; this generated pSHINE2192. Next, a PCR fragment containing the promoter sequence of the *spoVG* gene was amplified with the specific primer pair PspoVG-F (5′-GCCCGAA ATGAAAGCTTTATGA-3′) and PspoVG-R (5′-GCATTAG TGTATCAATTCCACG-3′). Genomic DNA of *B. subtilis* 168 (laboratory stock) was used as a template. The PCR fragment was introduced into the *Sma*I site of pSHINE2192 according to the TA-cloning method (*14*). The generated pSHINE2172 was then introduced into BEST2131 (*leuB*::pBRTc) (*15*), generating BEST12008. BEST12007 and BEST12005 were constructed by transforming UOT1317 (*sof1 spo0F*Δ) (*16*) and RIK3 (*spo0H*::pJ0H7d) (*17*, *18*), respectively, using pSHINE2172. BEST12013 was constructed as follows. The *cat* gene of pHASH102 (*14*) was PCR-amplified using the specific primer pair cat-F (5′-CAGTAATATTGACTT TTAAAAAAGGATTG-3′) and cat-R (5′-GAAACCATTATT ATCATGACATTAACC-3′) then introduced into the *Sma*I site of pRIK0Ed (*19*). This yielded plasmid pRIK0Ed-cat, which was introduced into the genomic DNA of 168, yielding BEST12013. To obtain BEST12014, BEST12013 was transformed using BEST12008 genomic DNA. BEST12025 was constructed as follows. The promoter of the *spo0E* gene was PCR-amplified with the specific primer pair Pspo0EF (5′-CCTGGGTATTGTTCTTCTAAT CCTATC-3′) and Pspo0ER (5′-GCTAAGAAATAGGAAAC AAGTTTGATTGGG-3′) then introduced into the *Sma*I site of pHASH103 (*14*), generating pST0E1. Next, the *spo0E* gene was amplified by PCR using the primer pair spo0ErandomF (5′-ATGNNNNNNNNNNNGGCGGTTC TTCTGAACAAGAAAGATTG-3′) and spo0ER (5′-GGCC GCTATTTATTTGCATCATATGC-3’) to attach the potential downstream elements that enhance translation efficiency (*20*). The fragment was introduced into the *Eco*RV site of pST0E1 and then introduced directly into the genomic DNA of BEST2131. Transformants with various sporulation frequencies appeared on plates containing chloramphenicol, erythromycin and tetracycline. A sporulation-defective mutant (BEST12022) was then isolated and the mutant *spo0E* gene was designated *spo0E102*. To generate BEST12026, BEST2136 (*leuB*::pBRTc *proB*::pBRBS *metB*::pBREm) (*15*) was transformed using the genomic DNA of BEST12008 and BEST12022. BEST12033 was generated by transforming BEST2131 using the pRIK0Ed-cat plasmid.

Sporulation Conditions—Bacillus subtilis cells were grown at 37°C in 2× SG medium containing 0.1% (w/v) D-glucose (*21*). To synchronize the growth phase of the cells, the culture was diluted 10-fold when the optical density at 660 nm (OD_{660}) reached 0.5. The end of the logarithmic growth phase (T_0) was defined as the point at which the culture reached an OD_{660} of 1.5.

Table 1. **Bacterial strains used in this study.**

Strain	Relevant genotype	Reference and notes
BEST2131	*spo0A* + *spo0E* + *spo0F* + *spo0H* + *leuB*::pBRTc	22
BEST12008	*spo0A* + *spo0E* + *spo0F* + *spo0H* + *leuB*::pBR::*erm*-P*spoVG-GFPuv*	This study
BEST12007	*sof1 spo0E* + *spo0F*Δ *spo0H* + *leuB*::pBR::*erm*-P*spoVG-GFPuv*	This study
BEST12005	*spo0A* + *spo0E* + *spo0F* + *spo0H*::pJ0H7d *leuB*::pBR::*erm*-P*spoVG-GFPuv*	This study
BEST12013	*spo0A* + *spo0E*::*cat spo0F* + *spo0H*+	This study
BEST12014	*spo0A* + *spo0E*::*cat spo0F* + *spo0H* + *leuB*::pBR::*erm*-P*spoVG-GFPuv*	This study
BEST12022	*spo0A* + *spo0E* + *spo0F* + *spo0H* + *leuB*::pBR::*cat*-P*spo0E-spo0E102*	This study
BEST12026	*spo0A* + *spo0E* + *spo0F* + *spo0H* + *metB*::*pBR*::*cat*-P*spo0E-spo0E102 leuB*::*pBR*::*erm*-P*spoVG-GFPuv proB*::*pBRBS*	This study
BEST12033	*spo0A* + *spo0E*::*cat spo0F* + *spo0H* + *leuB*::pBRTc	This study

The sporulation fraction was defined in terms of colony-forming units (CFU) per millilitre.

Microscopy and Data Processing—An aliquot (~20 μl) of culture medium at the sporulation phase was briefly centrifuged and the supernatant removed. Cells were washed once in MilliQ water then re-suspended in 2 μl of component A from the SlowFade-Antifade Kit (Molecular Probes, Inc., OR, USA). A 1 μl aliquot of the cell suspension was then inoculated onto an agarose layer on a glass slide and covered with a coverslip. Microscopic analyses were conducted using an AxioskopMOT 2 microscope (Carl Zeiss, Göttingen, Germany) and a CoolSNAP fx CCD camera (Roper Scientific, Inc., AZ, USA). To detect the fluorescence of GFPuv, Filter Set 17 (Carl Zeiss) was used. Images were obtained 40 s after UV excitation. The fluorescence intensity of individual cells was calculated using MetaMorph Ver. 4.6 software (Universal Imaging, Co., PA, USA).

Instrumentation—All capillary electrophoresis time-of-flight mass spectrometry (CE-TOFMS) experiments were performed using an Agilent CE Capillary Electrophoresis System G1600A (Agilent Technologies, CA, USA), and an Agilent TOFMS System G1969A. For system control and data acquisition we used G2201AA Agilent ChemStation software for CE and Analyst QS for Agilent TOFMS software.

CE-TOFMS Conditions for Cation Analysis—Samples were prepared as described in (*22*). Separations were carried out on a fused silica capillary (50 μm i.d. ×100 cm total length) using 1 M formic acid. Samples were injected with a pressure injection of 50 mbar for 3 s. The applied voltage was set at +30 kV and the sheath liquid was prepared as 50% (v/v) MeOH/H_2O. For TOFMS, ions were examined successively to cover the whole range of *m/z* values from 50 through 1,000. The fragmentor voltage was set at 75 V and the skimmer and Oct RFV voltages at 50 V and 125 V, respectively. The capillary voltage was set at 4,000 V (*23*).

CE-TOFMS Conditions for Anion/Nucleotide Analysis—Samples were prepared as described in (*22*). Separations were carried out on a fused silica capillary (50 μm i.d. ×100 cm total length) using 50 mM ammonium acetate (pH8.5 for anion, and pH7.5 for nucleotide, respectively). Samples were injected with a pressure injection of 50 mbar for 30 s. The applied voltage was set at +30 kV and the sheath liquid was prepared as 5-mM ammonium acetate 50% (v/v) MeOH/H_2O. For TOFMS, ions were examined successively to cover the whole range of *m/z* values from 50 through 1,000. The fragmentor voltage was set at 100 V and the skimmer and Oct RFV voltages at 50 V and 200 V for anion, and 75 V and 200 V for nucleotide, respectively. The capillary voltage was set at 3,500 V (*23*).

Data Processing—Peak extraction was carried out using our proprietary software (Sugimoto, unpublished data) and peak pre-processing was performed according to the P-BOSS method (*24*) using Excel 2003 (Microsoft, WA, USA). Mathematical simulation was conducted using XPP-AUTO (*25*). Statistical analyses were performed *via* MATLAB (Mathworks, MA, USA).

RESULTS AND DISCUSSION

The Negative-feedback Loop Dominates the Threshold of Sporulation Switch—In cells initiating sporulation, expression of *spo0H*, which encodes sporulation-specific σ^H, was induced by a reduction in the AbrB level (Fig. 1). The RNA polymerase that contains σ^H stimulated the expression of phosphorelay components, *kinA*, *spo0F* and *spo0A*, which constitute multiple points of the positive-feedback loop. Negative-feedback regulation was also observed in *B. subtilis* phosphorelay. Expression of the *spo0E* gene, which encodes Spo0A~P-specific phosphatase, is induced by a reduction in the AbrB level at the sporulation onset (*26*). Accordingly, it has been suggested that phosphorelay is negatively regulated by a solo feedback system (*27*).

A mathematical model was created, and the dynamics of the model were simulated (see Supplementary Data for detail). The system was characterized by varying two parameters, the sporulation signal (ϕ) and concentration of Spo0A~P, as illustrated in Fig. 2. The amount of stimulus required for sporulation switch increased as the ratio of negative and positive feedback loops, $r = f_N/f_P$, increased (Fig. 2A). Comparing the system characteristics by varying the feedback coefficients (f_N and f_P) revealed that as the value of f_N increased, the bistability region shifted its operating region dramatically towards a larger region against the sporulation signal (Fig. 2B), while f_P did not change its operating region sufficiently (Fig. 2C). These findings indicate that negative feedback, which is achieved by expression of the *spo0E* gene, primarily modulates bistability behaviour.

The function of Spo0E in population heterogeneity suggested in our mathematical model (Fig. 2A) was further demonstrated using BEST12014 (*spo0E*::*cat*), in which the negative-feedback loop created by *spo0E* is destroyed ($r = 0$ in our model). In this strain, distribution is excessively biased towards the sporulating subpopulation at T_3 (Fig. 3A and C), resulting in sporulation of >95% of the cells. This was consistent with the sporulation frequency at T_{24}. Next, we constructed a strain able

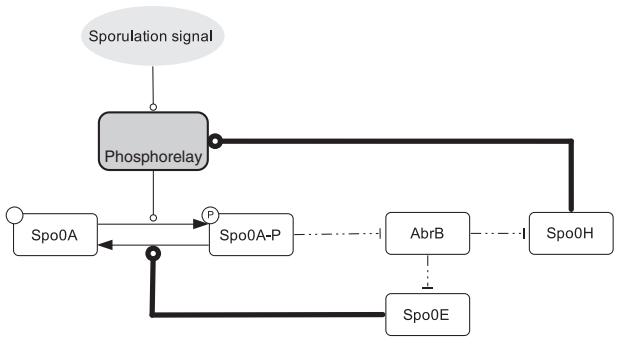

Fig. 1. **Schematic representation of the phosphorelay network required for initiation of sporulation in *B. subtilis*.** The diagram was illustrated using CellDesigner 3.5.1 (*37*) (http://celldesigner.org), and the notation follows that proposed by Kitano *et al*. (*38*). The networks downstream of AbrB are simply categorized into positive and negative feedback loops, the regulation of which is represented by a bold arrow from Spo0H, and a bold arrow from Spo0E, respectively.

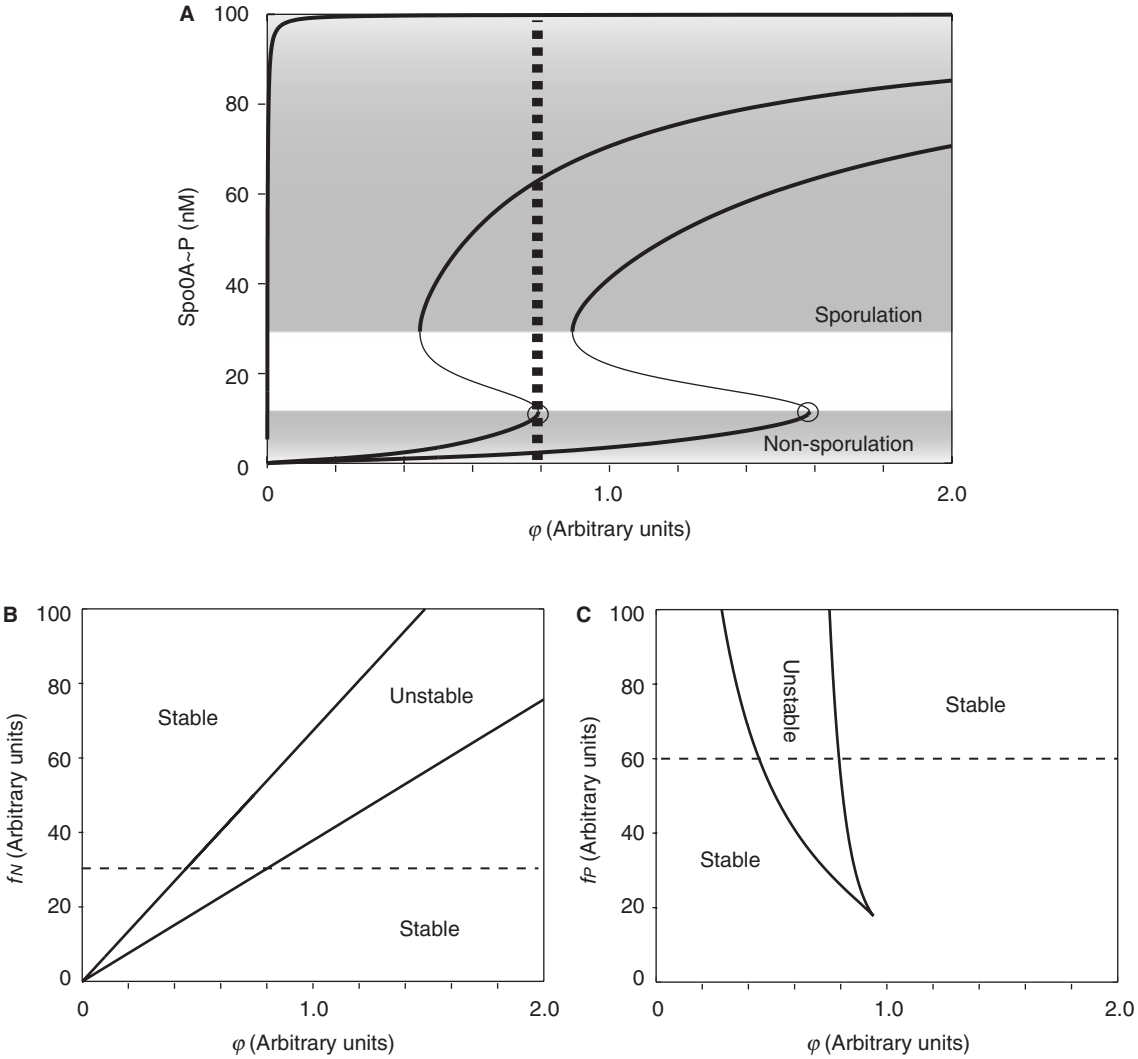

Fig. 2. **Behaviour of the sporulation-decision system as simulated using a mathematical model.** (**A**) Bifurcation diagram of the concentration of Spo0A~P against the sporulation signal. The curve in the middle represents characteristics under nominal parameter values, corresponding to the wild-type. The left side curve represents that obtained when negative feedback was completely removed; that is, $r = 0$. The right side curve represents that when the negative-feedback coefficient was doubled. The circle represents the threshold point of signal intensity and the two shaded regions the parameter space where cells underwent sporulation (upper region) or non-sporulation (lower region), which is dependent on the level of Spo0A~P. Given that the sporulation signal intensity is represented by a dotted line in the centre, the wild-type could yield either a low or high level of Spo0A~P, presumably *via* stochastic fluctuation of the signal (*39*). Removing negative feedback results in a consistently high level of Spo0A~P, whereas doubling the feedback results in a consistently lower level, yielding only sporulating/non-sporulating subpopulations, respectively. (**B** and **C**) A bifurcation diagram obtained by varying the sporulation signal and either feedback signal. Dotted lines indicate the parameter space of nominal values: (B) negative and (C) positive coefficient.

to produce a large amount of Spo0E protein (*spo0E*$^{++}$). Strain BEST12026 harbours a *spo0E102* mutation that contains an ideal ribosome-binding site and a strong downstream element (*20*). In BEST12026, the scale of the sporulating subpopulation at T_3 was <5% (Fig. 3B and D). These results were predicted in our mathematical model for phosphorelay (Fig. 2A) and indicate that negative-feedback regulation by Spo0E is a gearbox for modulating the sporulating subpopulation. We also confirmed, mathematically and experimentally, that heterogeneity during sporulation reflects a strategy for survival in fluctuating environmental conditions, unpublished data. To investigate molecular mechanisms upon sporulation, we use the above mutants so that either sporulating or non-sporulating populations could be examined.

Distinct Metabolome Profiles among Sporulation Stages—To investigate the effects of population heterogeneity on omics data, we demonstrated the variation of metabolome data in wild-type (*spo0E*$^{+}$), *spo0E*::*cat* (*spo0E*$^{-}$) and *spo0E102* (*spo0E*$^{++}$) strains. The detailed mechanisms and association between activities of the

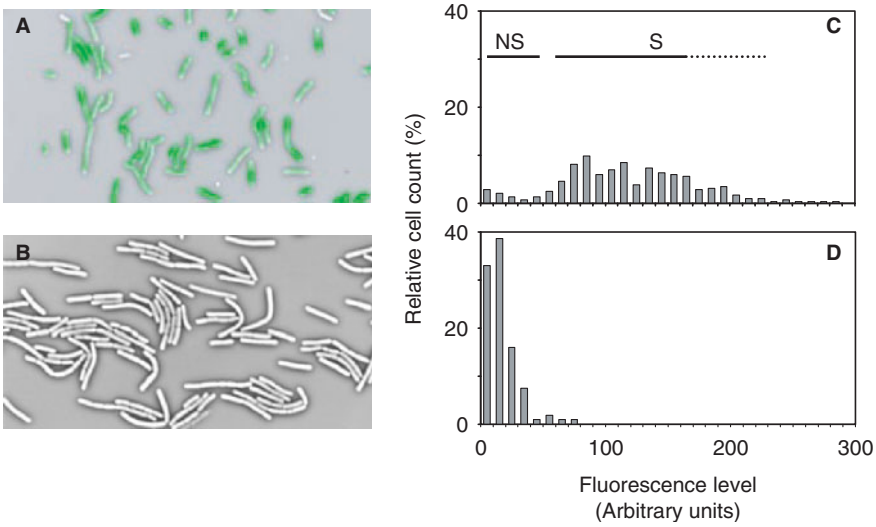

Fig. 3. **Effects of phosphorelay-associated mutations on the ratio of subpopulations generated at sporulation onset.** (**A** and **B**) Microscopic images of the population-distribution of phosphorelay-associated mutants. Wild-type and mutants harbouring the P_{spoVG}-*GFPuv* reporter gene were grown under sporulation conditions and observed under a microscope at T_3. Green fluorescence and phase-contrast images were inverted and overlaid. (**C** and **D**) Distribution of sporulating and non-sporulating subpopulations. The fluorescence intensity of single cells was measured under a fluorescence microscope. Histograms show fluorescence data obtained from more than 300 cells. (A and C) *spo0E*::*cat* (BEST12014), (B and D) *spo0E102* (BEST12022). NS and S indicate non-sporulating and sporulating subpopulations, respectively.

metabolic pathway and sporulation remain relatively unknown (*28*), compared with genetic and protein level analyses. All inactivating mutations in *B. subtilis* Krebs cycle genes cause a defect, and terminate at certain stages during sporulation [see (*29*) for a review]. Phosphorelay of Spo0A~P is thought to be controlled by the Krebs cycle, but a detailed metabolomics approach has yet to be performed. By comparing wild-type and *sdpC* knockout strains, Gonzalez-Pastor *et al*. (*30*) reported that ATP synthase is strongly expressed during sporulation. This suggests a link between energy metabolism and the sporulation signalling pathway. We previously conducted metabolome analysis in wild-type *B. subtilis*, confirming that most glycolysis metabolites are markedly decreased in the early stage of sporulation (*22*). However, we did not compare the metabolic profiles of sporulation-deficient strains, thus making it difficult to determine which pathways are critical or which metabolites are strongly correlated to sporulation activities. Recently, the relationships between branched-chain amino acids and CodY were revealed (*31–33*). CodY protein controls more than 100 genes that are induced when cells experience nutrient deprivation. GTP and isoleucine independently and additively increase the affinity of CodY towards its target sites, resulting in activation of its repressor function. To obtain more details on the metabolic profiles during sporulation, *i.e*. to obtain a better understanding of the metabolic pathway as a whole, we therefore conducted metabolome analysis based on CE-TOFMS (*22*).

We employed three strains carrying various *spo0E* alleles in their genomes: BEST2131 (wild-type), BEST12022 (*spo0E102*) and BEST12033 (*spo0E*::*cat*).

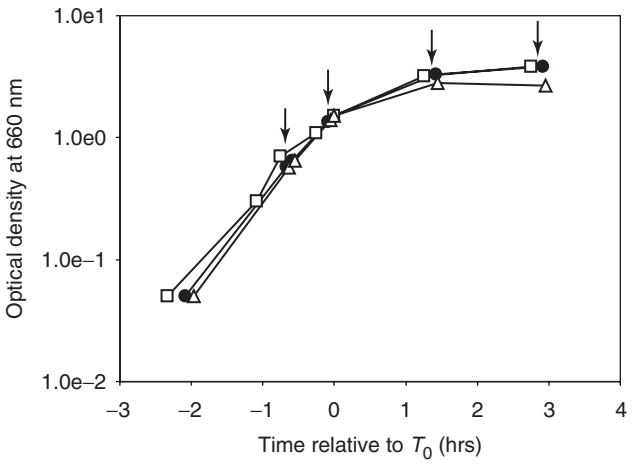

Fig. 4. **Growth curve of the examined strains.** Representative data from three samples is shown. *spo0E*+ (closed circles), *spo0E*::*cat* (open squares) and *spo0E102* (open triangles). Sampling points ($T_{-0.5}$, T_0, $T_{1.5}$, and T_3) are indicated by arrows.

The genetic background of these strains is *trpC2* and *leuB*::pBR, resulting in L-tryptophan and L-leucine auxotrophy. The growth characteristics of the strains were equivalent in 2x SG sporulation medium including 0.1% (w/v) of D-glucose (Fig. 4). Each strain was sampled at four time points, $T_{-0.5}$, T_0, $T_{1.5}$ and T_3, relative to the end of the logarithmic growth phase. These time points approximately correspond to the middle-logarithmic phase, transition phase, the time when the final symmetric septation is completed and the time when sporulation-specific asymmetric septation is completed in wild-type cells, respectively. We prepared metabolome

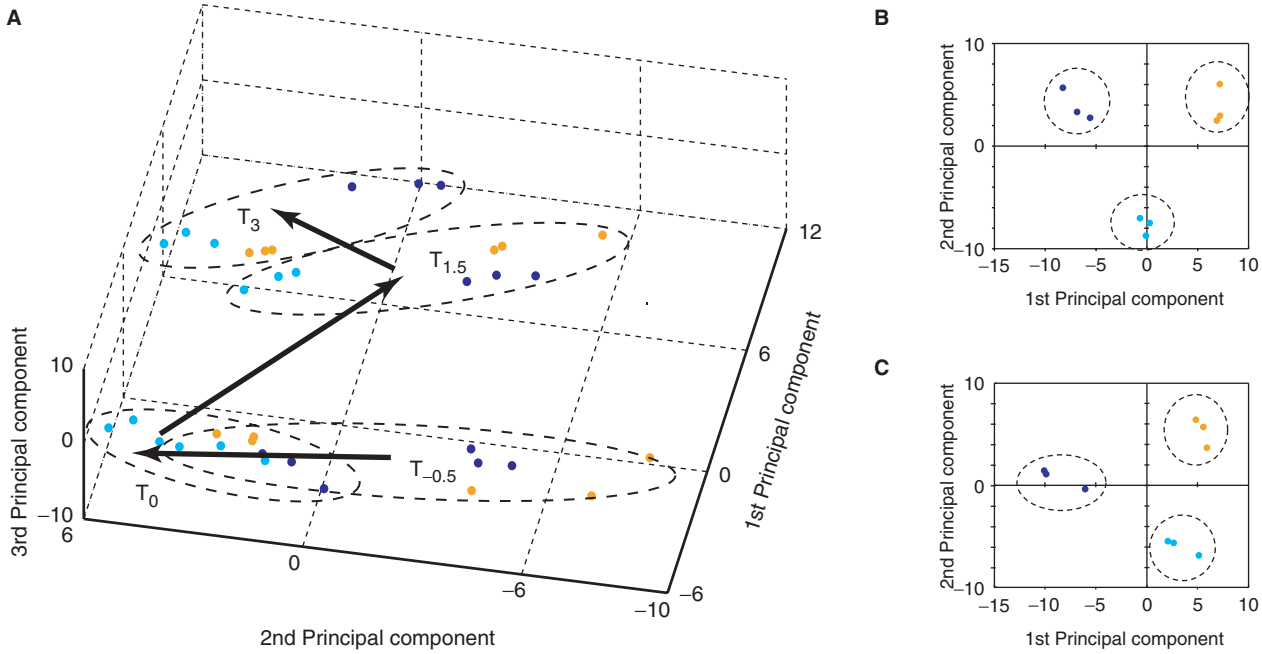

Fig. 5. **The metabolic state of sporulating *B. subtilis* based on PCA of the metabolome data.** (**A**) A three-dimensional principal component plot of the metabolome profiles of the sporulating *spo0E* variants ($n = 3$). Transition of the metabolic profiles of the three examined strains is indicated by arrows. (**B** and **C**) Two-dimensional principal component plots at $T_{1.5}$ (B) and T_3 (C). Dark blue, BEST2131 (*spo0E*$^+$); light blue, BEST12033 (*spo0E*::*cat*); orange, BEST12022 (*spo0E102*).

extracts and performed CE-TOFMS analysis (see MATERIALS AND METHODS section). To demonstrate whether each strain can be characterized independently by its metabolic profile, we performed PCA using the metabolome data, as is frequently conducted against omic data (*34*). We first selected the signals that were significantly different among the three strains by employing one-way analysis of variance (ANOVA) under a 5% significant level; it resulted in extracting 94 metabolites (Supplementary Table S2), which were then used for PCA. Due to aberrant peak shape, in some cases, our software cannot detect peaks, causing to have missing values. In order to avoid contamination of the missing peaks, the 94 peaks were extracted from the peaks which are automatically detected over all experiments, resulting in selection of peaks in a very strict manner. Improvement of software and measurement technology will have higher accuracy of peak extraction, and will lead to characterize metabolic profiles in more detail. As shown in Fig. 5A, the phase transitions could be clearly traced within the 3D principal component spaces. Intriguingly, we found that BEST12033 (*spo0E*$^-$) at $T_{-0.5}$ was not explicitly discriminated from that at T_0. This result indicates that the metabolic state during the logarithmic growth phase is similar to that at transition phase in BEST12033 (*spo0E*$^-$). This may be due to the function of Spo0E phosphatase not only at sporulation onset, but also in the logarithmic phase, *i.e.* Spo0A~P, which is slightly generated during the vegetative phase, is cancelled by the positively regulated *spo0E* product, inhibiting the initiation of sporulation. However, at present this hypothesis is no more than speculation. Because the cumulative contribution up to the third principal component was ~70%; up to the third principal component may not be still enough to capture the full characteristics of the sample. However, all other samples except BEST12033 (*spo0E*$^-$) exhibited distinct results at $T_{-0.5}$. As depicted in Fig. 5B and C, the three samples were clearly discriminated at $T_{1.5}$ and T_3, indicating that their metabolic states are clearly different at the onset of sporulation. We concluded that this was due to the population heterogeneity of sporulating wild-type cells; the metabolic profiles of wild-type cells may mislead our interpretation. To investigate the sporulating/non-sporulating subpopulations in a more distinct manner, we compare extreme cases hereafter (*i.e.* BEST12022 and BEST12033).

Energy Metabolism Exhibits Distinct Features Upon Sporulation—Sporulation is initiated by deprivation of nutrients such as carbon, nitrogen and phosphate sources. Further, under our experimental conditions, the glucose level in the medium was considered an important factor controlling the initiation of sporulation, since the addition of >0.5% (w/v) D-glucose efficiently inhibited sporulation (data not shown). We, therefore, expected glucose utilization pathways including glycolysis, the Krebs cycle and the pentose phosphate pathway to drastically fluctuate at sporulation onset. The overall metabolome profiles are depicted in Supplementary Fig. S3. Intracellular levels of metabolic intermediates, especially fructose-1,6-bisphosphate (F1,6P) and acetyl CoA, were reduced upon sporulation onset (Supplementary Fig. S3). This suggests that the glycolysis pathway is activated during growth phase by the aggressive use of glucose. This is consistent with the data obtained in our previous report (*22*).

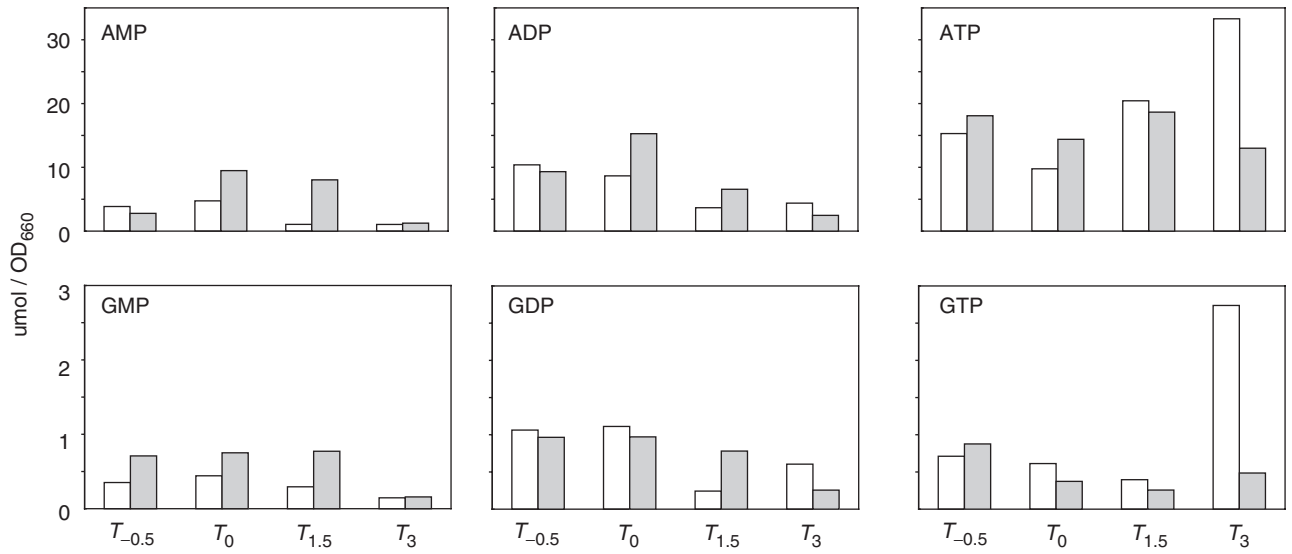

Fig. 6. **Metabolic profiles of nucleotides.** White bars, BEST12033. Grey bars, BEST12022.

Significant differences were observed in lactic acid levels between the two *spo0E* variants. In BEST12033 (*spo0E*$^{-}$), the intracellular level was higher than that in BEST12022 (*spo0E*$^{++}$) throughout cultivation, suggesting that trace amounts of Spo0A∼P accumulated in vegetative BEST12033 (*spo0E*$^{-}$) cells likely activate the glycolysis pathway. In the Krebs cycle, on the other hand, different profiles were obtained for intermediate metabolites (Supplementary Fig. S3). In particular, the metabolism pathway seemed significantly altered after the initiation of sporulation. In both *spo0E* variants, citrate levels were drastically increased after T_0, but not generated until T_0. This observation suggests that the Krebs pathway, which is dormant during the logarithmic growth phase, is activated at stationary phase when environmental glucose is spent. Behaviour of the downstream pathway of citrate was also different between the two strains; 2-oxoglutararic acid was highly accumulated in sporulating BEST12033 (*spo0E*$^{-}$). This result suggests that metabolism, at least that involving 2-oxoglutaric acid in the Krebs cycle, is required for metabolic differentiation towards sporulation. Inactivation of citrate synthase and aconitase, which catalyse this metabolism, results in a sporulation-deficient phenotype at early stages of sporulation (*29*). Nitrogen metabolism is also considered a key factor in sporulation, because the pathway from 2-oxoglutaric acid to glutamine via glutamic acid is the solo acceptor of ammonium ions. Metabolite levels of glutamine, as well as that of purines, were also shown to increase after $T_{1.5}$. The downstream metabolites of 2-oxoglutaric acid, succinic acid, fumaric acid and malic acid, were highly accumulated in stationary BEST12022 (*spo0E*$^{++}$). This observation suggests that the latter pathway of the Krebs cycle is blocked or rapidly circulated in sporulating BEST12033 (*spo0E*$^{-}$).

Changes in the Energy Charge State During Sporulation—In sporulating BEST12033 (*spo0E*$^{-}$), we could not decide whether or not the latter steps of the Krebs cycle were activated. If activated, ATP should be generated by an electron transfer system using NAD(P)H. We, therefore, determined the levels of phosphorylated adenosine (AXP) during sporulation (Fig. 6 and Supplementary Fig. S3).Unexpectedly, sporulating cells (BEST12033, *spo0E*$^{-}$) exhibited a dramatic increase in ATP levels, while non-sporulating cells (BEST12022, *spo0E*$^{++}$) decreased its level after $T_{1.5}$. These results strongly support the data of Gonzalez-Pastor *et al*. (*30*) who showed, from a metabolite viewpoint, that ATP synthase is strongly expressed upon sporulation. It was previously reported that ATP remains approximately constant during the sporulation process; however, this conclusion was based on the outcomes of observations using a wild-type strain, which generates heterologous culture of both sporulating and non-sporulating cells. If these distinct features discriminate between sporulating/non-sporulating cells, our results suggest that this past study presented the average results of both subpopulations, thus cancelling out the sporulation/non-sporulation effect.

Levels of phosphorylated guanosines (GXP) were also determined (Fig. 6 and Supplementary Fig. S3) since a decrease in GTP is thought to trigger sporulation (*35*). We observed a decrease in GTP at T_0, as well as a decrease in inosine-5′-phosphate (IMP) at the same time. The GTP level increased at T_3 only in BEST12033 (*spo0E*$^{-}$), supporting ATP production at the onset of sporulation. This result indicates that sporulating cells accumulate energy to prepare for the energy-consuming process of spore formation. Intriguingly, several nucleotides (AMP, ADP, GMP and GDP) increased transiently at T_0 in both strains. It would therefore be interesting to examine whether their transient activities, in addition to that of GTP, are linked to the initiation of sporulation.

Most Amino Acids are Independent of the Sporulation Process—All amino acids except for cysteine, which was under the detection limit, were categorized according to

Table 2. **Characterization of amino acids.**[a]

Amino acid[b]	BEST12033	BEST12022	Pathway category
Ser	I	V	Glycolysis
Val	I	IV	Glycolysis
Ala	II	II	Glycolysis
Gly	IV	IV	Glycolysis
His	I	I	Pentose
Phe	IV	IV	Pentose
Tyr	IV	IV	Pentose
Asp	IV	I	Krebs
Gln	IV	I	Krebs
Pro	IV	V	Krebs
Arg	III	III	Krebs
Asn	I	I	Krebs
Ile	II	II	Krebs
Lys	IV	IV	Krebs
Met	IV	IV	Krebs
Thr	II	II	Krebs
Glu	V	V	Krebs

[a]Each amino acid was categorized into one of the following five classes depending on the time series profiles. I: increase during sporulation transition followed by a decrease; II: decrease; III: decrease during sporulation transition followed by an increase; IV: increase; and V: no change. Amino acids exhibiting different profiles are highlighted in grey.
[b]Leu and Trp were excluded because the strains harbour *trpC* and *leuB*::*pBR* mutations.

their transition characteristics. The results are summarized in Table 2. Most amino acids exhibited similar characteristics when comparing the two strains. An association between branched-chain amino acids (*e.g*. isoleucine, leucine and valine) and CodY, a GTP-binding protein, has been shown (*36*). In BEST12033 (*spo0E*$^{-}$), valine (but not isoleucine) exhibited distinct characteristics compared with BEST12022 (*spo0E*$^{++}$). That is, its level increased transiently at T_0 then dropped again, which is consistent with the finding that CodY directly targets its biosynthesis (*31–33*). Asparagine and glutamine are nitrogen-rich amino acids and central components of nucleic acid production. It is suggested that in combination with the nucleotide results, *i.e*. the massive generation and thus accumulation, the increased levels of these amino acids may be attributed to sporulation preparation.

CONCLUSIONS

We investigated the mechanism of heterogeneity during sporulation in wild-type *B. subtilis*. Using simulation and modelling techniques, we found that negative feedback is a primary modulating factor in the bistability of sporulation, which is directly affected by the *spo0E* gene. We then confirmed these results experimentally by deleting/over-expressing *spo0E*. The findings mathematically support the proposals suggested in previous reports (*7*), and suggest that population heterogeneity should be considered in omics studies including transcriptomics, proteomics and metabolomics. In addition, we also examined the sporulation stages by metabolome analysis. To investigate the sporulating and non-sporulating stages in a distinct manner, we used the mutants mentioned above (*i.e*. BEST12033 and BEST12022) and compared transition of metabolite levels. As a result, we found that metabolism was significantly different among each stage regardless of whether the population was sporulating or non-sporulating. Although we need to further investigate each metabolite in detail, this study provides enormous information suggesting links between metabolome activities and spore formation. The inclusion of additional mutants (such as *spo0A*) will provide further insight into the molecular mechanisms of sporulation as well as cell differentiation.

Supplementary Data are available at *JB* online.

We are grateful to Yasuhiro Naito, Rintaro Saito and Kotaro Oka for discussions and suggestions. We also thank Hideyuki Ohshima, Seira Nakamura, Gin Maeta, Yuji Sakakibara and Masatomo Hirabayashi for technical assistance.

REFERENCES

1. Balaban, N.Q., Merrin, J., Chait, R., Kowalik, L., and Leibler, S. (2004) Bacterial persistence as a phenotypic switch. *Science* **305**, 1622–1625
2. Maamar, H. and Dubnau, D. (2005) Bistability in the *Bacillus subtilis* K-state (competence) system requires a positive feedback loop. *Mol. Microbiol.* **56**, 615–624
3. Ozbudak, E.M., Thattai, M., Lim, H.N., Shraiman, B.I., and Van Oudenaarden, A. (2004) Multistability in the lactose utilization network of *Escherichia coli*. *Nature* **427**, 737–740
4. Chung, J.D. and Stephanopoulos, G. (1995) Studies of transcriptional state heterogeneity in sporulating cultures of *Bacillus subtilis*. *Biotechnol. Bioeng.* **47**, 234–242
5. Chung, J.D., Stephanopoulos, G., Ireton, K., and Grossman, A.D. (1994) Gene expression in single cells of *Bacillus subtilis*: evidence that a threshold mechanism controls the initiation of sporulation. *J. Bacteriol.* **176**, 1977–1984
6. Grossman, A.D. (1995) Genetic networks controlling the initiation of sporulation and the development of genetic competence in *Bacillus subtilis*. *Annu. Rev. Genet.* **29**, 477–508
7. Veening, J.W., Hamoen, L.W., and Kuipers, O.P. (2005) Phosphatases modulate the bistable sporulation gene expression pattern in *Bacillus subtilis*. *Mol. Microbiol.* **56**, 1481–1494
8. Burbulys, D., Trach, K.A., and Hoch, J.A. (1991) Initiation of sporulation in *B. subtilis* is controlled by a multicomponent phosphorelay. *Cell* **64**, 545–552
9. de Jong, H., Geiselmann, J., Batt, G., Hernandez, C., and Page, M. (2004) Qualitative simulation of the initiation of sporulation in *Bacillus subtilis*. *Bull. Math. Biol.* **66**, 261–299
10. Smits, W.K., Kuipers, O.P., and Veening, J.W. (2006) Phenotypic variation in bacteria: the role of feedback regulation. *Nat. Rev. Microbiol.* **4**, 259–271
11. Voigt, C.A., Wolf, D.M., and Arkin, A.P. (2005) The *Bacillus subtilis* sin operon: an evolvable network motif. *Genetics* **169**, 1187–1202
12. Iber, D. (2006) A quantitative study of the benefits of co-regulation using the spoIIA operon as an example. *Mol. Syst. Biol.* **2**, 43
13. Iber, D., Clarkson, J., Yudkin, M.D., and Campbell, I.D. (2006) The mechanism of cell differentiation in *Bacillus subtilis*. *Nature* **441**, 371–374

14. Ohashi, Y., Ohshima, H., Tsuge, K., and Itaya, M. (2003) Far different levels of gene expression provided by an oriented cloning system in *Bacillus subtilis* and Escherichia coli. *FEMS Microbiol. Lett.* **221**, 125–130
15. Itaya, M. (1993) Integration of repeated sequences (pBR322) in the *Bacillus subtilis* 168 chromosome without affecting the genome structure. *Mol. Gen. Genet.* **241**, 287–297
16. Hoch, J.A., Trach, K., Kawamura, F., and Saito, H. (1985) Identification of the transcriptional suppressor sof-1 as an alteration in the spo0A protein. *J. Bacteriol.* **161**, 552–555
17. Jaacks, K.J., Healy, J., Losick, R., and Grossman, A.D. (1989) Identification and characterization of genes controlled by the sporulation-regulatory gene spo0H in *Bacillus subtilis*. *J. Bacteriol.* **171**, 4121–4129
18. Ohashi, Y., Sugimaru, K., Nanamiya, H., Sebata, T., Asai, K., Yoshikawa, H., and Kawamura, F. (1999) Thermo-labile stability of sigmaH (Spo0H) in temperature-sensitive spo0H mutants of *Bacillus subtilis* can be suppressed by mutations in RNA polymerase beta subunit. *Gene* **229**, 117–124
19. Nanamiya, H., Fugono, N., Asai, K., Doi, R.H., and Kawamura, F. (2000) Suppression of temperature-sensitive sporulation mutation in the *Bacillus subtilis* sigA gene by rpoB mutation. *FEMS Microbiol. Lett.* **192**, 237–241
20. Ohashi, Y., Yamashiro, A., Washio, T., Ishii, N., Ohshima, H., Michishita, T., Tomita, M., and Itaya, M. (2005) In silico diagnosis of inherently inhibited gene expression focusing on initial codon combinations. *Gene* **347**, 11–19
21. Leighton, T.J. and Doi, R.H. (1971) The stability of messenger ribonucleic acid during sporulation in *Bacillus subtilis*. *J. Biol. Chem.* **246**, 3189–3195
22. Soga, T., Ohashi, Y., Ueno, Y., Naraoka, H., Tomita, M., and Nishioka, T. (2003) Quantitative metabolome analysis using capillary electrophoresis mass spectrometry. *J. Proteome Res.* **2**, 488–494
23. Soga, T., Baran, R., Suematsu, M., Ueno, Y., Ikeda, S., Sakurakawa, T., Kakazu, Y., Ishikawa, T., Robert, M., Nishioka, T., and Tomita, M. (2006) Differential metabolomics reveals ophthalmic acid as an oxidative stress biomarker indicating hepatic glutathione consumption. *J. Biol. Chem.* **281**, 16768–16776
24. Morohashi, M., Shimizu, K., Ohashi, Y., Abe, J., Mori, H., Tomita, M., and Soga, T. (2007) P-BOSS: A new filtering method for treasure hunting in metabolomics. *J. Chromatogr A.* (in press)
25. Ermentrout, B. (2002) Simulating, Analyzing, and Animating Dynamical Systems SIAM Press, Philadelphia
26. Perego, M. and Hoch, J.A. (1991) Negative regulation of *Bacillus subtilis* sporulation by the spo0E gene product. *J. Bacteriol.* **173**, 2514–2520
27. Perego, M. and Hoch, J.A. (2002) Two-component systems, phosphorelays, and regulation of their activities by phosphatases in *Bacillus subtilis* and its closest relatives: from genes to cells (Sonenshein, A.L., Hoch, J.A., and Losick, R., eds.)pp. 473–481 ASM Press, Washington DC
28. Dworkin, J. and Losick, R. (2001) Linking nutritional status to gene activation and development. *Genes Dev.* **15**, 1051–1054
29. Sonenshein, A. L. (2002) The Krebs citric acid cycle in *Bacillus subtilis* and its closest relatives: from genes to cells (Sonenshein, A.L., Hoch, J.A., and Losick, R., eds.) ASM Press, Washington D.C.
30. Gonzalez-Pastor, J. E., Hobbs, E. C., and Losick, R. (2003) Cannibalism by sporulating bacteria. *Science* **301**, 510–513
31. Ratnayake-Lecamwasam, M., Serror, P., Wong, K.W., and Sonenshein, A.L. (2001) *Bacillus subtilis* CodY represses early-stationary-phase genes by sensing GTP levels. *Genes Dev.* **15**, 1093–1103
32. Shivers, R.P. and Sonenshein, A.L. (2004) Activation of the *Bacillus subtilis* global regulator CodY by direct interaction with branched-chain amino acids. *Mol. Microbiol.* **53**, 599–611
33. Sonenshein, A.L. (2005) CodY, a global regulator of stationary phase and virulence in Gram-positive bacteria. *Curr. Opin. Microbiol.* **8**, 203–207
34. Raamsdonk, L.M., Teusink, B., Broadhurst, D., Zhang, N., Hayes, A., Walsh, M.C., Berden, J.A., Brindle, K.M., Kell, D.B., Rowland, J.J., Westerhoff, H.V., van Dam, K., and Oliver, S.G. (2001) A functional genomics strategy that uses metabolome data to reveal the phenotype of silent mutations. *Nat. Biotechnol.* **19**, 45–50
35. Beaman, T.C., Hitchins, A.D., Ochi, K., Vasantha, N., Endo, T., and Freese, E. (1983) Specificity and control of uptake of purines and other compounds in *Bacillus subtilis*. *J. Bacteriol.* **156**, 1107–1117
36. Molle, V., Nakaura, Y., Shivers, R.P., Yamaguchi, H., Losick, R., Fujita, Y., and Sonenshein, A.L. (2003) Additional targets of the *Bacillus subtilis* global regulator CodY identified by chromatin immunoprecipitation and genome-wide transcript analysis. *J. Bacteriol.* **185**, 1911–1922
37. Funahashi, A., Morohashi, M., Tanimura, N., and Kitano, H. (2003) CellDesigner: a process diagram editor for gene-regulatory and biochemical networks. *BIOSILICO* **1**, 159–162
38. Kitano, H., Funahashi, A., Matsuoka, Y., and Oda, K. (2005) Using process diagrams for the graphical representation of biological networks. *Nat. Biotechnol.* **23**, 961–966
39. Maughan, H. and Nicholson, W.L. (2004) Stochastic processes influence stationary-phase decisions in *Bacillus subtilis*. *J. Bacteriol.* **186**, 2212–2214